Investigation of Magnetic Field and Radial Force Harmonics in a Hydrogenerator Connected to a Three-Level NPC Converter

Mostafa Valavi, Arne Nysveen, and Roy Nilsen
Department of Electric Power Engineering
Norwegian University of Science and Technology (NTNU)
Trondheim, Norway
mostafa.valavi@ntnu.no

***Abstract*—This paper investigates spatial and time harmonics of flux density and radial force distributions in the airgap of a hydrogenerator with fractional-slot windings. Hydrogenerator is connected to a neutral-point-clamped (NPC) converter, representing a converter-fed synchronous machine (CFSM) in pumped-storage hydropower plant. Magnetic field in the hydrogenerator is computed using time-stepping finite element (FE) analysis, coupled with an external circuit (where PWM converter is modelled). Radial forces are calculated analytically based on Maxwell stress tensor. Three loading conditions are studied (i.e. resistive loading and converter-fed operation with two different carrier frequencies). In the paper, it is investigated how converter-fed operation could change the characteristics of the radial magnetic forces. It is also discussed how vibration of the hydrogenerator is expected to be affected by additional harmonics generated by the PWM converter.**

***Keywords*—Hydrogenerator, fractional-slot windings, NPC converter, radial forces, vibration, pumped-storage hydro.**

I. INTRODUCTION

Variable-speed operation of hydropower plants (more specifically pumped-storage plants) can be beneficial for power system and for the hydropower plant itself [1-3]. As an energy storage technology, variable-speed pumped-storage plants can improve the integration of renewables into the power system. Due to variable-speed capability, stability and control of the power system can be enhanced. In the hydropower plant, rotational speed of the generator does not need to be constant and can be adjusted to improve the hydraulic efficiency and to reduce vibration and cavitation problems. To realize variable-speed operation, the following two configurations can be utilized: doubly fed induction machine (DFIM), and converter-fed synchronous machine (CFSM). While CFSM has many advantages over DFIM [1, 4], its drawback is the need for a full-rated converter. In DFIM configuration, the rating of the converter is reduced (around 30% of rated power). Because of this, DFIM has been the preferred technology for high power ratings [2, 5]. However, due to the advancement in the field of semiconductor devices and converter topologies, it is expected that CFSM will be available for increasingly higher power ratings. The largest installed CFSM has been in operation since 2013 in Grimsel 2 pumped-storage plant [6, 7]. In CFSM configuration, the synchronous generator/motor is connected to the grid via a full-rated back-to-back voltage source converter, as shown in Fig. 1.

TABLE I
SPECIFICATIONS OF HYDROGENERATOR AND CONVERTER

Generator	Power	105 MVA
	Speed	428.6 rpm
	Number of poles	14
	Number of slots	180
	Airgap diameter	3672 mm
	Machine length	1800 mm
Converter	Configuration	3-level NPC
	Switches	Ideal
	PWM	Sinusoidal
	Carrier frequency	450 Hz, 1050 Hz

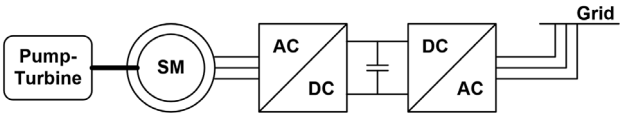

Fig. 1. CFSM configuration in a pumped-storage hydropower plant.

Converter-fed operation of the hydrogenerator could potentially bring new challenges, due to the increased harmonic content. In this paper, based on finite element (FE) analysis, both space and time harmonics in magnetic field and radial force distributions are investigated for a hydrogenerator connected to a three-level neutral-point-clamped (NPC) converter. The generator under investigation is a 180-slot/14-pole salient-pole machine with fractional-slot windings. It is connected to a NPC converter with ideal switches and sinusoidal PWM. Three loading cases are included in the analysis; resistive loading and converter-fed operation with 450 Hz (9 times fundamental frequency of 50 Hz) and 1050 Hz (21 times fundamental frequency) as the carrier frequency. Table I shows the specifications of the converter-fed synchronous machine.

The paper is organized as follows: FE modeling and simulations are discussed in Section II. In Section III, magnetic field distribution is analyzed. Section IV includes the analysis of

This work was supported by Norwegian Hydropower Centre (NVKS) and Norwegian Research Centre for Hydropower Technology (HydroCen).

radial forces, as one of the main causes of stator vibration. Concluding remarks are presented in Section V.

II. Time-Stepping FE Simulations

In order to have access to both time and space distributions of the magnetic field, time stepping FE analysis is employed where field data of the hydrogenerator is stored in a series of time instants. NPC converter is modeled in an external circuit coupled with the FE simulation, as shown in Fig. 2. As can be seen in the figure and compared with Fig. 1, only AC/DC (i.e. machine-side) converter is modeled and the DC link capacitors are replaced by DC voltage sources. For the hydrogenerator, damper bars are not modeled. The reason is that for a CFSM configuration, the generator does not necessarily need to be equipped with the dampers since the transient operation can be controlled by the power electronic converter. However, it should be noted that damper bars must be provided if CFSM configuration includes a bypass switch for direct connection of the generator to the grid (converter is bypassed in this case).

Due to the inclusion of the PWM converter, time step of the simulations is chosen to be sufficiently small (i.e. 10 μs). The magnetic flux density distribution in the airgap is stored every 100 μs and is used for the harmonic analysis of the magnetic field and radial forces.

In the FE simulations, the hydrogenerator supplies either resistive loads or NPC converter. In the case of NPC converter, two carrier frequencies (450 Hz and 1050 Hz) are studied. For all three loading cases, generator current amplitude and torque angle are kept the same, in order to have a meaningful comparison.

Line voltage, DC current and 3-phase currents of the generator are shown in Fig. 3, for the case of generator connected to NPC converter (1050 Hz). As it is clear in the figure, the generator terminal currents contain much less additional harmonics induced by converter-fed operation compared with the terminal voltages. This is due to the relatively large inductance of the electrical machine. As mentioned earlier, damper bars are not modeled in the synchronous generator under study. With inclusion of dampers, the phase currents would have a higher harmonic content, due to the contribution from the damper leakage inductances.

Time harmonic content of the terminal voltage and current are shown in Fig. 4 (normalized based on the fundamental 50 Hz component). The harmonic orders are identical for both current and voltage. However, the amplitude of the voltage harmonics is significantly higher. It is also evident that the amplitude of the harmonics are increased in the case of a lower carrier frequency, as expected. When generator supplies resistive loads, the harmonic content is very low, including multiples of the fundamental frequency (i.e. 5th, 7th, etc.). In the case of converter-fed operation, the dominant harmonics in generator current are determined by $f_{sw} \pm 2f_e$ and $f_{sw} \pm 4f_e$, where f_{sw} and f_e (= 50 Hz) are carrier frequency and fundamental frequency, respectively. Those are 850 Hz, 950 Hz, 1150 Hz and 1250 Hz (when f_{sw} is equal to 1050 Hz) and 250 Hz, 350 Hz, 550 Hz, and 650 Hz (when f_{sw} is equal to 450 Hz). The harmonics in the generator current will induce additional flux

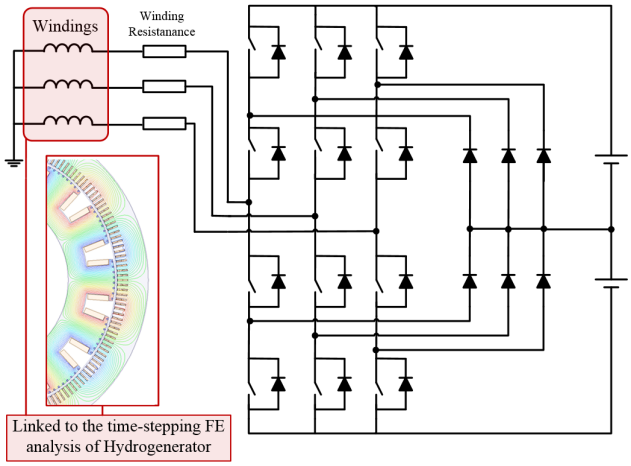

Fig. 2. Coupled circuit (NPC converter) linked to the FE simulations.

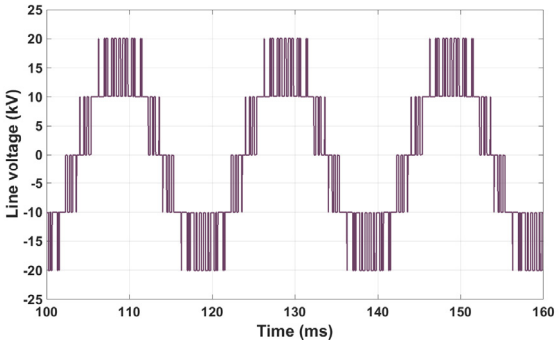

(a)

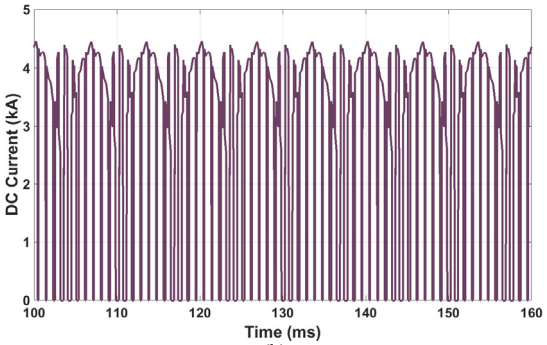

(b)

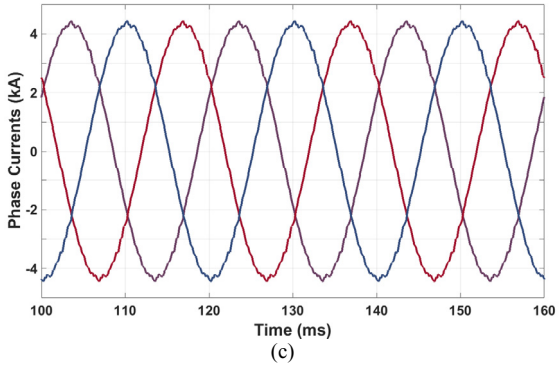

(c)

Fig. 3. NPC-1050 Hz case: (a) Line-to-line voltage at the generator terminal. (b) Output DC current in the top branch. (c) Generator 3-phase currents (NPC-1050 Hz).

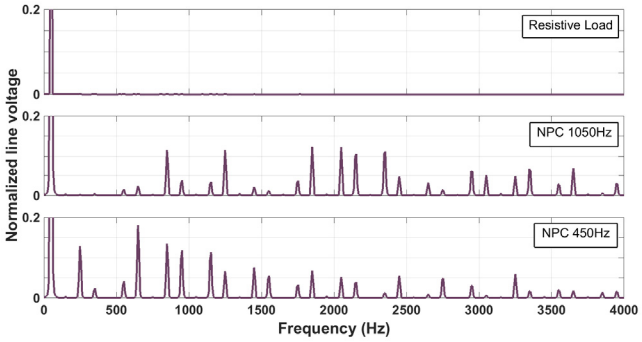

(a)

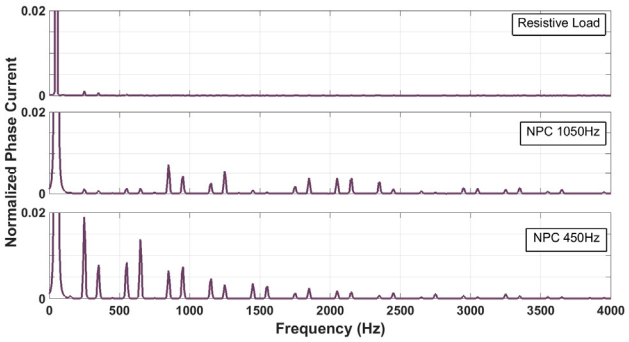

(b)

Fig. 4. Time harmonic content for different loading cases: (a) Generator terminal voltage. (b) Generator terminal current.

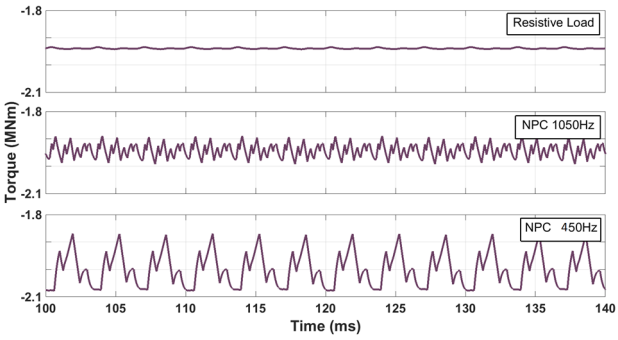

(a)

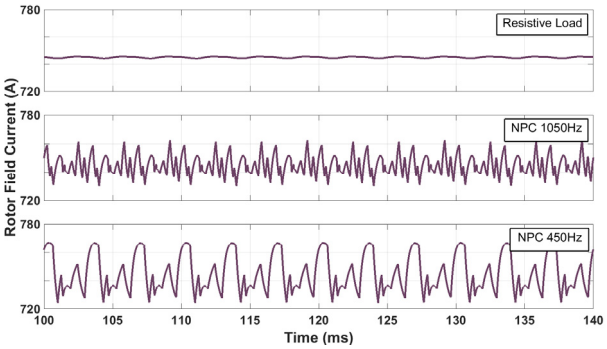

(b)

Fig. 5. (a) Generator electromagnetic torque. (b) Generator rotor field current.

density waves which are of interest in this paper. For f_{sw}= 1050 Hz, the amplitude of the largest current harmonic ($f_{sw} - 4f_e$=850 Hz) is less than 1% of fundamental component. This ratio increase in the case of f_{sw}=450 Hz, where amplitude of the largest harmonic ($f_{sw} - 4f_e$=250 Hz) is about 2% of the fundamental component.

Electromagnetic torque waveform is presented in Fig. 5 (a) for different loading conditions. According to the figure, for a resistive load, torque is very smooth, containing $6f_e$ and $12f_e$ components. However, their amplitude is very small and torque ripple is about 0.5%. As can be seen in the figure, converter fed operation adds additional harmonics to the electromagnetic torque. Torque ripple is increased to 5.1% (f_{sw}=1050 Hz) and 10.5% (f_{sw}=450 Hz). The main harmonic component in the torque waveform is 900 Hz (for f_{sw}=1050 Hz) and 300 Hz (for f_{sw}=450 Hz) and equal to $f_{sw} - 4f_e + f_e$. It is produced by the interaction between the main rotor field component (f_e) and largest harmonic in the stator current ($f_{sw} - 4f_e$), which creates a MMF field harmonic with the same harmonic order.

The rotor field winding of the hydrogenerator is supplied with a DC current that is shown in Fig. 5 (b). Due to the flux density harmonics (caused by stator current harmonics, not rotating with the same speed as rotor), a ripple is induced in the DC rotor current. According to this figure, the ripple is significantly larger in the case of converter-fed operation and is largest when carrier frequency is lower. The ripple is 0.2% for the case of resistive load and increases to 4.2% (f_{sw}=1050 Hz) and 5.6% (f_{sw}=450 Hz) for converter-fed operation. The harmonic orders in the rotor current are similar to the torque harmonics, as they are similarly produced by the interaction between rotor and stator flux density waves.

III. Analysis of Magnetic Field

In this section, flux density spatial distribution in the airgap is studied in various time steps. This makes it possible to investigate both time and space harmonics. At load conditions, airgap magnetic field is formed by the interaction between rotor field and magnetomotive force (MMF) produced by the stator 3-phase currents. In converter-fed operation, generator currents contain additional time harmonics, which leads to creation of additional time harmonics in the airgap flux density. The analysis here aims to reveal the space and time characteristics of the flux density waves when generator is connected to the PWM converter.

Spatial harmonic orders of radial flux density at one time instant in the case of resistive loading are presented at Fig. 6. The order of the main spatial harmonic component is 7, which corresponds to the number of pole pairs (p). Spatial harmonics with orders equal to odd multiples of pole pair number (21st, 35th, 49th, etc.) also have a considerable amplitude. Spatial slot harmonics are 173th and 187th harmonics and their orders can be determined based on $N_s \pm p$, where N_s is the slot number.

If time-varying flux density is plotted at one point in the airgap (not shown here due to the lack of space), the main frequency would be 50 Hz which is equal to the fundamental

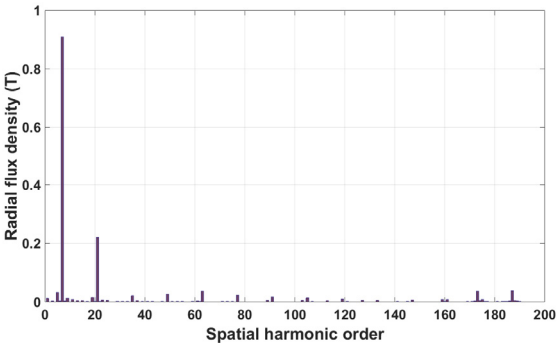

Fig. 6. Spatial harmonic orders of airgap flux density at one time instant in the case of resistive loading.

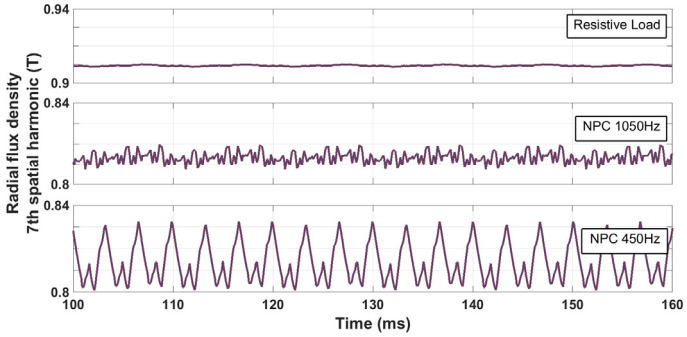

Fig. 7. Time-varying amplitude of the 7th spatial harmonic of radial flux density.

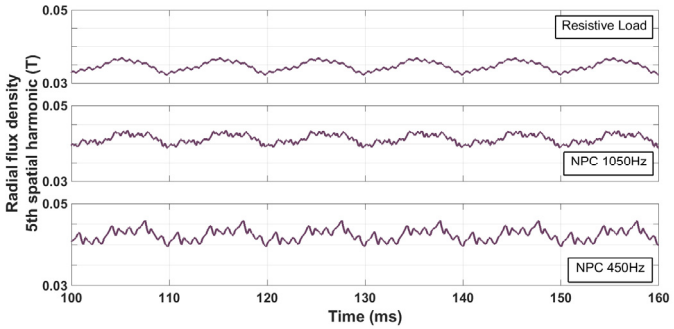

Fig. 8. Time-varying amplitude of the 5th spatial harmonic of radial flux density.

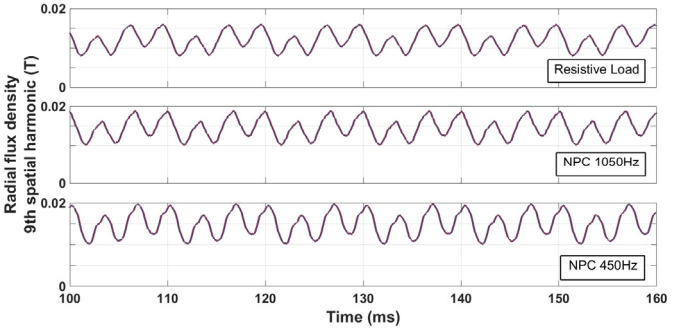

Fig. 9. Time-varying amplitude of the 9th spatial harmonic of radial flux density.

frequency. The main frequency of the main spatial harmonic (7th) is also expected to be 50 Hz, since it is rotating synchronized with the rotor itself and induces a 50 Hz voltage and in the stator windings. As mentioned earlier, converter-fed operation could create additional time harmonics in the flux density waves. Therefore, it is expected to see other time harmonics, in addition to the 50 Hz component, in the characteristics of the main 7th spatial harmonic. It means that there might be various flux density waves with pole number equal to 7, but with different rotational speeds. This could be the case for the other spatial harmonics as well.

In this paper, in order to investigate different time harmonics of a flux density spatial harmonic the following method is employed: the amplitude of one spatial harmonic (e.g. 7th) is computed over time. If the amplitude is constant then it means that there is only one flux density wave with that pole number and a specific speed. Main frequency component of this flux wave can be identified using the computed phase shift of the spatial harmonic. If the resulting amplitude is varying with time, this indicates that there are additional flux density waves with different rotational speeds. In this case, the frequency spectrum of time-varying amplitude can reveal the order of the additional time harmonics. This method can be used for the analysis of both flux density (this section) and force density (next section) waves.

Fig. 7 shows the time-varying amplitude of the flux density main 7th harmonic. As can be seen in the figure, in the case of resistive loading, the amplitude is almost constant. As expected, converter-fed operation create additional flux density harmonics and as a result, the amplitude is varying with time. Variations are considerably larger in the case of 450 Hz carrier frequency, where ripple is about 4%. Computed phase shift of the 7th harmonic reveals that for all loading cases, the main frequency component is 50 Hz, as expected. Frequency spectrum of the time-varying amplitude (not presented here) shows that the largest additional frequency components in the main spatial harmonics are 850 Hz (for f_{sw}=1050 Hz) and 250 Hz (f_{sw}=450 Hz). As mentioned before, these two component are the largest additional time harmonics in stator current ($f_{sw} - 4f_e$) and are produced by the PWM converter.

As will be discussed in the next section, the most important spatial flux density harmonic from vibration perspective are 5th, 7th and 9th. Therefore, time-varying amplitude of 5th and 9th harmonics are also investigated and presented in Fig. 8 and Fig. 9. It is evident that for both spatial harmonics, in contrast to the main 7th harmonics, the amplitude has considerable variations even in the case of resistive loading and converter-fed operation does not greatly change its characteristics. The ripple in the amplitude of the 5th is about 12% for all loading cases. For 9th spatial harmonics, ripple increases to as large as 60% for all loading cases. Computation of the phase shifts shows that while the main frequency component is 50 Hz for the 5th harmonic, it is equal to 150 Hz for the 9th harmonic. A sub-harmonic with the spatial order of 1 can also be seen in the figure. For hydrogenerator with fractional-slot windings, sub-harmonics (spatial harmonics with orders lower than main component) exist in the flux density distribution. The spatial order of the lowest subharmonic is equal to GCD (N_s, p), i.e. the greatest common divisor of the number of pole pairs and the number of slots.

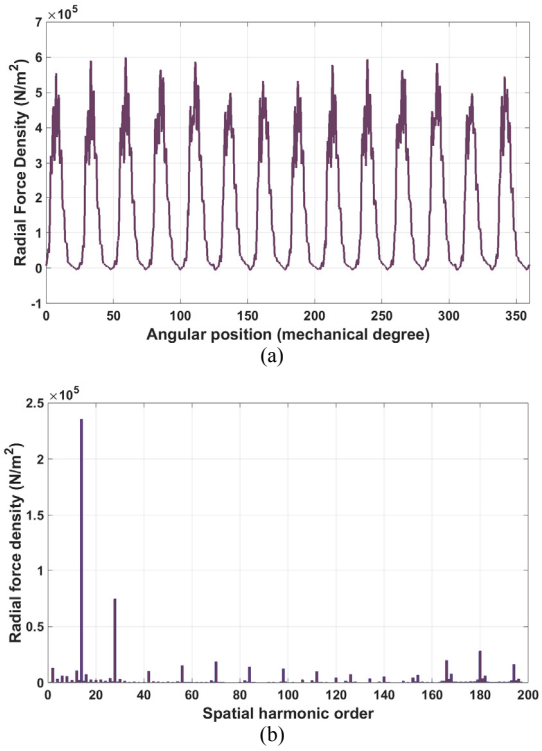

Fig. 10. Radial force density at one time instant. (a) Spatial distribution. (b) Spatial harmonc orders.

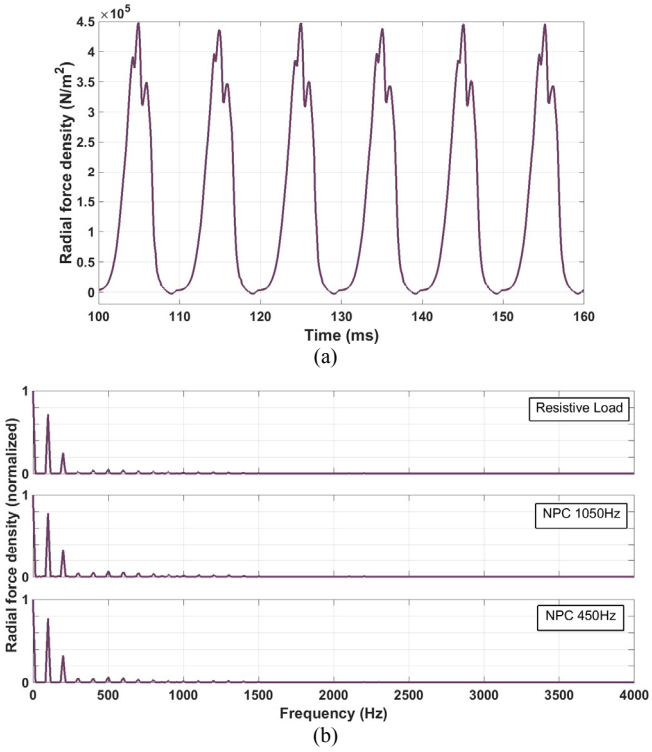

Fig. 11. Radial force density at one point in the airgap. (a) Variation with time. (b) Time harmonics.

IV. Analysis of Radial Forces

Radial forces acting on stator teeth are among the main causes of vibration in electrical machines. These forces are produced between rotor and stator, by the interaction between flux density waves. Maxwell's stress tensor is used to calculate radial force density in the airgap:

$$f_r = \frac{1}{2\mu_0}\,(B_r^2 - B_t^2) \tag{1}$$

where B_r and B_t denote radial and tangential airgap flux density. Since both space and time distribution of the flus density is computed using time-stepping FE analysis, it is possible to investigate spatial and temporal characteristics of the radial forces, based on (1). A radial force density wave, as a function of both space and time, can be expressed as:

$$f_r(\theta, t) = F_{rm} \cos\,(m\theta - k\omega t - \varphi_F) \tag{2}$$

where θ and t are angular mechanical position and time. m and k denote spatial and temporal harmonics, respectively. ω and φ_F are angular velocity and phase. These radial force waves act on stator teeth, cause deformation in the stator and produce vibration. The amplitude of the deformations in the stator (when resonance is neglected) is inversely proportional to m^4[8]. This means that lowest non-zero spatial orders can cause largest deformations and are most important from vibration perspective.

Fig. 10 shows spatial distribution of the radial force density at one time instant, together with its spatial harmonic orders. As it is clear in both Fig. 10 (a) and (b), the main spatial component is the 14th (i.e. pole number). According to (1), the order of the main force density component is expected to be twice the order of the main flux density component (i.e. pole pair number). Despite having the largest amplitude, the spatial order of the 14th harmonic (m=14) is too high for producing considerable vibration. The 2nd spatial harmonic (m=2) of force density has the lowest order and hence is most important from vibration point of view. Fig. 11 (a) shows how radial force density at one point in the airgap varies with respect to time. Time harmonic spectrum is presented at Fig. 11 (b). As can be seen in the figure, the main frequency component is 100 Hz and equals twice the main frequency component of flux density (i.e. 50 Hz), based on (1). Multiples of 100 Hz are also present in the spectrum, including a 200 Hz harmonic with a considerable amplitude. According to the figure, time-varying radial force density at one point is very similar for all loading cases and is not affected by converter-fed operation. However, for a comprehensive analysis, time varying radial force density must be investigate along the complete airgap and not only one point. In this case, both space and time characteristics of different radial force waves can be revealed.

The aim of this section is to determine how converter-fed operation could potentially change the vibration level of the hydrogenerator. For this purpose, time-varying amplitude of the 2nd and 4th radial force density harmonics (lowest non-zero spatial orders) are investigated. In addition, the time-varying mean value of radial force density distribution is studied (0th spatial order) as it can produce 0th mode of vibration.

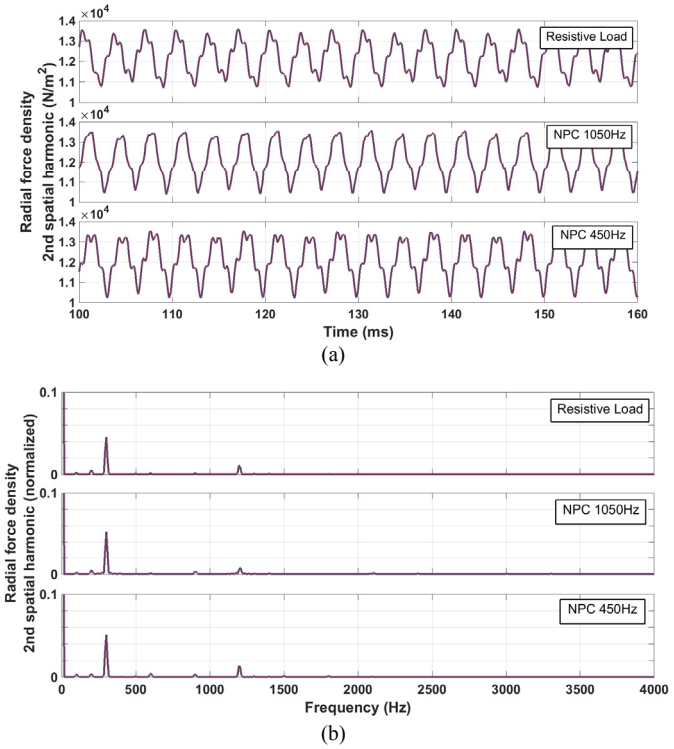

Fig. 12. (a) Time-varying amplitude of the 2nd spatial harmonic of radial force density. (b) Time harmonic content.

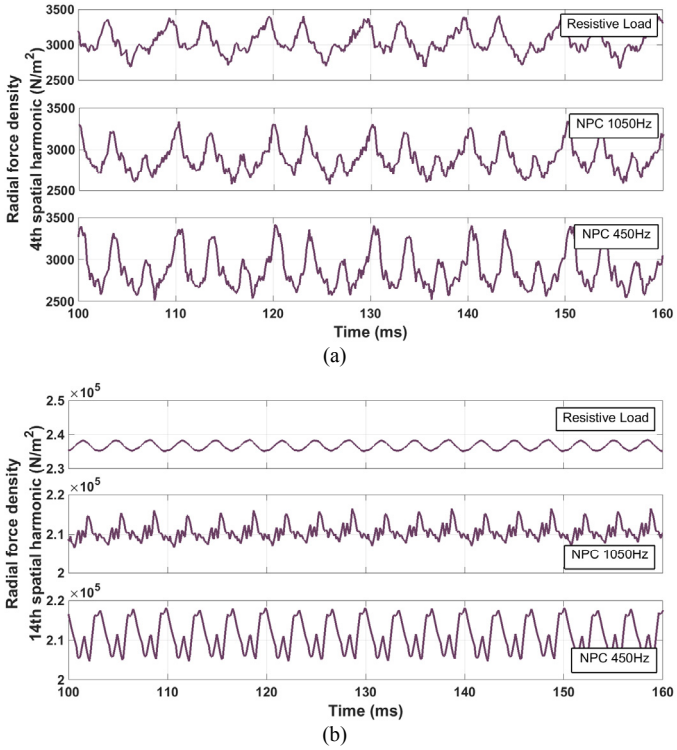

Fig. 13. Time-varying amplitude of spatial harmonics in radial force density distribution. (a) 4th harmonic. (b) 14th harmonic.

For the analysis of radial forces, the same method described in Section III is employed. Time-varying amplitude of the 2nd, 4th and 0th (mean value) spatial harmonics of radial force density is investigated. Time harmonic content of the amplitude reveals the additional temporal harmonics having the same spatial order. Moreover, the main frequency component of each spatial harmonic can be identified using its phase shift.

Time-varying amplitude of the 2nd spatial harmonic of radial force density and its harmonic content is shown in Fig. 12. This radial force wave is the most important cause of vibration in the hydrogenerator, producing a 2nd mode of vibration. Based on this figure, the amplitude, its variation, and also harmonic content are not considerably affected by the converter-fed operation. The ripple (around 25% for all loading cases), exists even in the case of resistive load and is not caused by PWM converter. Based on (1) and using flux density harmonics presented in Fig. 6, the amplitude of the 2nd radial force harmonic can be calculated as:

$$f_r(2^{nd}) = \frac{1}{2\mu_0}\left[\frac{1}{2}B_{r1}^2 + \sum_{n=1,2,3}^{\infty} B_{rn}\,.\,B_{r(n+2)}\right] \quad (3)$$

where B_{rn} is the amplitude of the n-th spatial harmonic of radial flux density. According to (3), the 2nd force spatial harmonic is produced by the interaction between flux density spatial harmonics whose orders differ by two and also by 1st spatial harmonic (i.e. lowest order sub-harmonic). According to the amplitude of different flux density harmonics (shown in Fig. 6), it is evident that 2nd radial force harmonic is mainly produced by the interaction between two pairs of flux density harmonics: 5th and 7th and also 7th and 9th. The reason is that even though 5th and 9th harmonics have a relatively small amplitude, their product with large amplitude of the 7th harmonic ($B_{r5} \times B_{r7}$ and $B_{r7} \times B_{r9}$) is by far the largest contributor in (3). According to Fig. 7-9, (where time-varying amplitude of these three harmonics are depicted) shows that the normalized variations in B_{r5} and B_{r9} are significantly larger than B_{r7}. As a result, variations in $B_{r5} \times B_{r7}$ and $B_{r7} \times B_{r9}$ are mainly due to the ripples in B_{r5} and B_{r9} (which does not depend on converter-fed operation), rather than B_{r7} (affected by converter harmonics). This is why characteristics of the 2nd radial force harmonic, and consequently vibration due to the 2nd mode, are not affected by converter-fed operation.

Based on time-varying phase shift of the 2nd radial force spatial harmonic, its main frequency component is 100 Hz. Frequency spectrum of the amplitude (presented in Fig. 12 (b)) revels that there is an additional radial force wave with same spatial order (m=2), but with a frequency of 200 Hz. This 200 Hz component can also be seen in Fig. 11, with a considerable amplitude.

Fig. 13 (a) shows the time-varying amplitude of the 4th spatial harmonic in radial force density. As depicted in the figure, this harmonic, similar to the 2nd mode, is not affected considerably by converter-fed operation. Similarly, the other low-order radial force density harmonics (i.e. 6th and 8th) are not affected considerably by converter harmonics. On the other hand, the variation in the amplitude of the largest component in

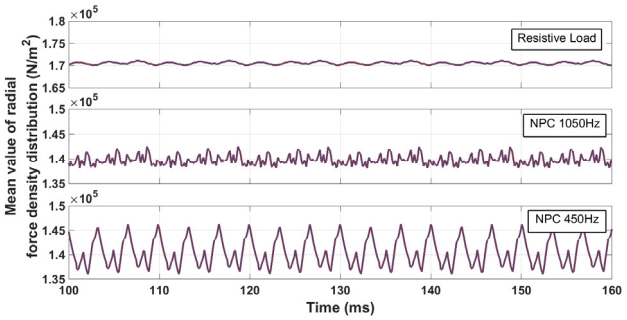

Fig. 14. Time-varying mean value of radial force density distribution.

radial force density distribution (i.e. 14th) is increased in the case of converter-fed operation, as shown in Fig. 13 (b). The reason is that this harmonic is mainly produced by the main 7th component of flux density, which is affected by converter harmonics. As mentioned earlier, the spatial order of this largest force component (i.e. 14) is too high to produce vibration. Therefore, for the generator under investigation, vibration due to the non-zero lowest modes is not expected to change considerably. However, it should be noted that converter-fed operation will induce additional frequency components in the radial force waves and this could potentially increase the chance of resonance vibration.

In addition to the non-zero low-order radial force harmonics, 0-th order radial force (i.e. variation in the mean value of radial force density distribution with respect to time) can produce 0-mode of vibration. It is produced by the interaction between flux density waves of same spatial order but with different time harmonics. Due to additional converter harmonics, it is reasonable to expect a larger 0-th order radial force component in the case of converter-fed operation. Fig. 14 shows the time-varying mean value of radial force density distribution. As expected, the variations are larger when generator supplies a PWM converter. While the ripple is about 0.6% in the case of resistive loading, it increases to 3% and 7.5% for 1050 Hz and 450 Hz converter-fed operation.

V. Conclusion

In this paper, operation of a hydrogenerator connected to a PWM converter is investigated using time-stepping FE analysis coupled with an external circuit. The paper aims to study the effects of converter harmonics on airgap flux density and radial force density harmonics. It is shown that among the spatial flux density harmonics, the main component (spatial order is equal to pole pair number) is most affected by converter-fed operation. It is found that non-zero lowest-order radial force harmonics (e.g. 2nd and 4th) are not considerably influenced by PWM converter. Therefore, influence of converter harmonics on vibration due to these modes is expected to be insignificant. Analysis of the 0-th order radial force component reveals that it is noticeably affected in the case converter-fed operation. Similarly, electromagnetic torque is also affected and torque ripple considerably increases. In general, it is shown that when generator supplies PWM converter, radial force waves would contain additional frequency components. This could potentially affect the resonance vibration in the hydrogenerator. It is concluded that the amplitude of additional time harmonics are larger in the case of lower carrier frequency, which leads to a greater influence on radial forces and vibration.

References

[1] M. Valavi, A. Nysveen, "Variable-speed operation of hydropower plants: past, present, and future," in *Proc. ICEM*, 2016, pp. 640-646.

[2] "Modeling and analysis of value of advanced pumped storage hydropower in the United States," Argonne National Laboratory, 2014.

[3] R. J. Kerkman, T. A. Lipo, W. G. Newman, J. E. Thirkell, "An inquiry into adjustable speed operation of a pumped hydro plant- part 1: machine design and performance," *IEEE Trans. Power Apparatus and Systems*, pp. 1828-1837, September/October 1980.

[4] P. K. Steimer, O. Senturk, S. Aubert, S. Linder, "Converter-fed synchronous machines for pumped hydro storage plants," in *Proc. ECCE*, 2014, pp. 4561-4567.

[5] A. Bocquel, J. Janning, "Analysis of a 300 MW variable speed drive for pump-storage plant applications," in *Proc. EPE Conference*, 2005, pp. 1-10.

[6] H. Schlunegger and A. Thöni, "100 MW full-size converter in the Grimsel 2 pumped-storage plant," in *Proc. Hydro*, 2013.

[7] "Grimsel 2: the world's largest power converter for variable speed pumped hydropower," *ABB Case Note*, available online.

[8] M. Valavi, A. Nysveen, R. Nilssen, R. D. Lorenz, T. Rolvag, "Influence of pole and slot combinations on magnetic forces and vibration in low-speed PM wind generators," *IEEE Trans. Magnetics*, vol. 50, no. 5, May 2014.